International Journal of GEOMATE, Dec., 2025 Vol.29, Issue 136, pp.1-10
ISSN: 2186-2982 (P), 2186-2990 (O), Japan, DOI: https://doi.org/10.21660/2025.136.5237
Geotechnique, Construction Materials and Environment

MODEL EXPERIMENTS ON FAILURE MECHANISM OF VOLCANIC SLOPES DURING SEISMIC LOADING AND RAINFALL

Ryuta Komatsu[1], Thanh An Nguyen[1], Motohiro Suzuki[2], *Shima Kawamura[1] and Yuta Izumi[1]

[1]Graduate School of Engineering, Muroran Institute of Technology, Japan; [2]Koken Engineering Co., Ltd., Japan

*Corresponding Author, Received: 22 Sep. 2025, Revised: 10 Nov. 2025, Accepted: 17 Nov. 2025

ABSTRACT: This study aims to clarify the mechanical behavior until failure of slopes formed from pyroclastic fall deposits (Tarumae volcanic soil: Ta-d) in Atsuma Town, Hokkaido, Japan, under seismic loading and rainfall conditions. Experiments utilized highly fragile Ta-d PR layer samples for the model slopes. The experiment used a model soil container with a one-dimensional cyclic loading apparatus for seismic loading tests and a spray nozzle system to make it rain artificially. Instrumentation consisted of pore water pressure gauges, dielectric soil moisture sensors, and accelerometers. Particle breakage of soils was quantified by measuring the fine content increase rate (ΔFc) via sieve analysis of samples before and after testing. Shaking table tests revealed that strong seismic loading caused an increase in pore water pressure, resulting in slope failure, even at low saturation. Crushing of soil particles was confirmed under seismic loading, indicating that cyclic shearing in volcanic coarse-grained soils can induce particle breakage and lead to earthquake-induced slope instability. Rainfall tests showed that slopes failed due to infiltration, with pore water pressure and moisture changes varying by initial water content. Particle crushing of soils was also observed during rainfall, more so in wetter conditions. A unique relationship was found between initial and failure-time water content, consistent with other volcanic soils in Hokkaido. These findings offer fundamental data for predicting slope collapse and suggest practical stability assessment via field measurements.

Keywords: Pyroclastic fall deposits, Earthquake, Rainfall, Model experiments, Slope stability

1. INTRODUCTION

Pyroclastic soils, also called volcanic soils, are found worldwide. In Japan, they cover around 40% of Hokkaido's total area [1-2]. These soils originate from pyroclastic materials erupted from volcanoes [1] and are considered “problematic” in geotechnical engineering due to their complex and often misunderstood characteristics, making them difficult to classify as conventional sandy or clayey soils [2-3]. Consequently, their complex mechanical and physical properties have attracted significant research interest. In particular, Miura et al. (2003) characterized the static and cyclic deformation-strength properties of volcanic coarse-grained soils, including particle fragmentation, based on site investigations employing standard penetration test (SPT), cone penetration test (CPT), and seismic cone penetration test (SCP) [4]. Hyodo et al. (2022) investigated the mechanical properties of Shirasu, a volcanic soil for Kagoshima Prefecture, using drained and undrained monotonic and cyclic triaxial compression tests [5]. Matsumura et al. (2023) investigated the replication of porous and non-porous particles exhibiting equivalent morphological characteristics (form, waviness, and texture) by 3D printing technology [6].

The study of the dynamic response of geotechnical structures under seismic loading is significant and encompasses a broader scope than just the basic soil properties. It is challenging to understand how foundations behave during earthquakes. Al-Ameri et al. (2020) presented an unbiased proof that parameters such as soil-to-structure stiffness ratio, thickness of the soil layer beneath, and duration of seismic events affect both vertically and horizontally [7]. Jawad et al. (2021) performed a finite element analysis of a zoned earth dam, revealing that higher upstream water levels, along with the degree of saturation and the void ratio of the clay core material, dramatically affect key factors, including water flux, hydraulic conductivity, and the peak displacement under seismic loads [8].

Recent earthquakes and excessive rain in Japan have caused much damage to the land, especially to natural slopes, cut slopes, and embankments. This has led to a lot of research on how volcanic soil slopes fail when things like rainfall, earthquake and freeze-thaw actions happen. Goto (1993) investigated freeze-thaw induced disruption in Toyoura sand and sand-fines mixtures through laboratory tests [9]. Ishikawa and Miura (2011) assessed the impact of freeze-thaw cycles on the deformation-strength properties of crushable volcanic coarse-grained soils, revealing considerable particle breakage at relatively low stress levels and saturated conditions through monotonic triaxial compression tests [10]. Matsumura et al. (2015) investigated the impact of freeze-thaw cycles on the cyclic shear characteristics of a crushable volcanic soil prevalent in Hokkaido using newly developed cyclic triaxial equipment [11]. Kawamura et al. (2013, 2021) have significantly advanced the

understanding of slope behavior under rainfall, freeze-thaw cycles, and their combined effects. Their 2013 study utilized small-scale model slopes, employing spray nozzles and shaking tables to simulate rainfall and cyclic loading, revealing environmental factors' influence on slope stability in cold regions like Hokkaido [1]. Subsequently, their large-scale model experiment (reported in 2021) confirmed the effectiveness of a previously developed prediction method for rainfall-induced collapse [12]. Recently, Nguyen et al. (2022) conducted 1g model experiments on slopes using Komaoka volcanic coarse-grained soils in Hokkaido, Japan. Their study examined the durability of embankments during post-rainfall earthquakes and clarified the effects of fine content on their mechanical behavior under individual rainfall and earthquake loading conditions [2, 13]. Kawamura et al. (2024) recently elucidated the geotechnical properties of the less-explored pyroclastic fall deposits (Ta-d), noting their minimal coverage in existing research and their unique characteristics, such as a pronounced strength decrease under low stress and high particle crushability compared to other volcanic soils in Hokkaido [3].

The present study investigates the mechanical behavior during earthquakes and rainfall using a model slope composed of Ta-d from Atsuma Town, originating from Mt. Tarumae's eruption. This aligns with previous studies on volcanic soils from the Kashiwabara (from the Shikotsu Caldera), Komaoka, and Tōhoro regions (the latter from the Mashū Caldera) in Hokkaido, Japan [1, 12]. Furthermore, we compare the relationship between initial and failure-time water contents proposed in previous studies [1-2] with that of volcanic soils in Hokkaido, aiming to collect fundamental data for predicting slope failure.

2. RESEARCH SIGNIFICANCE

This research provides original experimental insights into the coupled effects of seismic loading and rainfall on the stability of slopes composed of pyroclastic fall deposits (Tarumae volcanic soil: Ta-d). Unlike previous studies focusing separately on earthquake or rainfall impacts, this study uniquely integrates both conditions using physical model slope experiments. The novelty lies in quantifying particle breakage through the fine content increase rate (ΔFc) and establishing a distinctive relationship between initial and failure-time water content. The findings reveal the mechanism of slope failure under combined dynamic and hydrological effects, offering new perspectives for predicting volcanic soil slope instability in field applications.

3. TEST EQUIPMENT AND SPECIMENS

For this study, pyroclastic fall deposits (Ta-d), which are believed to have been ejected and deposited approximately 9,000 years ago from Mt. Tarumae, were sampled from the vicinity of the Hidaka Horonai River in Horonai, Atsuma Town, Yufutsu District, Hokkaido (Fig. 1), located approximately 5 km from the earthquake epicenter, and used in the experiments. As shown in Fig. 2, in the Hidaka Horonai River basin, the following layers were identified from the outcrop surface downwards: ① Ta-d reddish-brown layer (Ta-d PR layer) at 80 cm-135 cm depth, ② Ta-d fine pumice layer (Ta-VY layer) at 135 cm-140 cm depth, and ③ Ta-d pumice layer (Ta-d PG layer) at 140 cm-180 cm depth. Ta-d PR and Ta-d VY are extremely fragile and can be crushed with a finger to release the water retained in soil particles, which have a muddy appearance. A series of model tests was conducted using samples taken from the Ta-d PR layer.

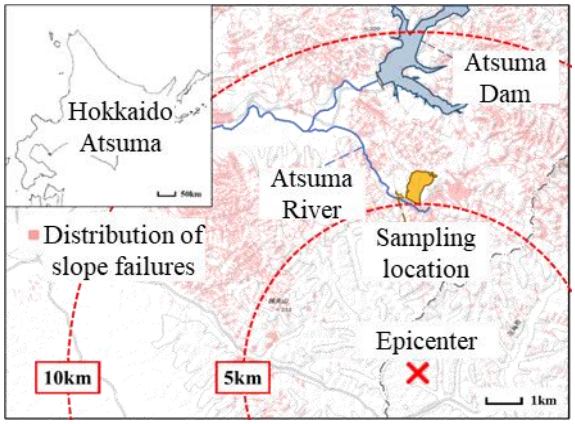

Fig. 1 Sampling location

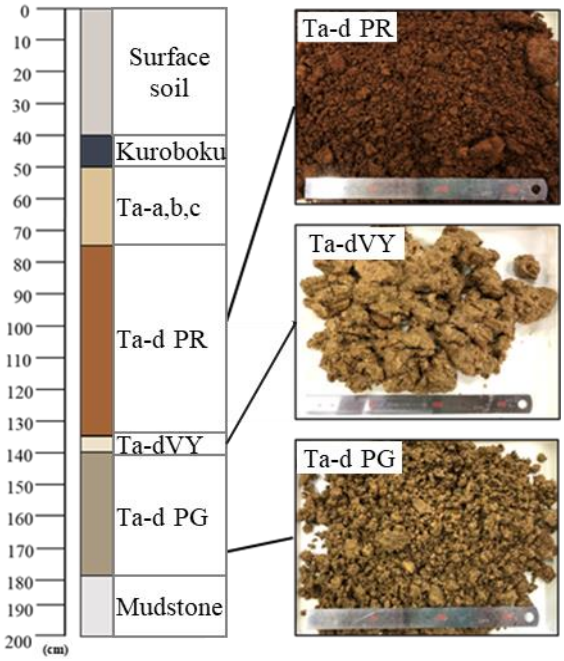

Fig. 2 Stratigraphic column

Figure 3 and Table 1 present the physical properties of the soil. While the average ignition loss (LOI) of volcanic soils in Hokkaido is known to be approximately 10% or less, the high LOI observed in Ta-d is attributed to an increase in structural crystalline water resulting from weathering. This is supported by the fact that halloysite is also included in the Ta-d soil composition. Further details are available in the previously reported paper [3].

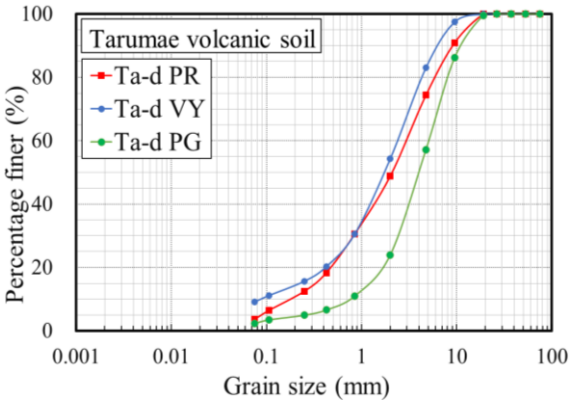

Fig. 3 Grain size distribution of Ta-d

Table 1. Physical properties

Natural water content, w_n (%)	144.6
Particle density, ρ_s (g/cm³)	2.740
In-situ dry density, $\rho_{d\ in\text{-}situ}$ (g/cm³)	0.442
Minimum dry density, $\rho_{d\ min}$ (g/cm³)	0.429
Maximum dry density, $\rho_{d\ max}$ (g/cm³)	0.602
Liquid limit, w_L (%)	Non-Plastic
Plastic limit, w_p (%)	Non-Plastic
Loss on ignition (%)	11.5
Mean grain size, D_{50} (mm)	2.9
Uniformity Coefficient, Uc	5.1

Figure 4 shows the overall diagram of the testing apparatus used in this study. The model soil tank, which has internal dimensions of 2,000 mm in width, 700 mm in height, and 600 mm in depth, is equipped with drainage ports at the bottom so that drainage conditions can be maintained in the experiments. A one-dimensional cyclic loading device (shaking table dimensions: 400 mm in length, 450 mm in height, 580 mm in depth) is attached to it. A 20 mm-thick tempered glass is installed on the front, allowing observation of the slope's deformation behavior. Seismic loading is computer-controlled using a hydraulic cylinder, enabling a maximum amplitude of ±50 mm, and regular waves (sine waves) with frequencies from 0.05 Hz to 5.0 Hz to achieve the target acceleration (495 gal, 540 gal and 600 gal). Artificial rainfall is reproduced by spraying from a nozzle installed at a height of 2.6 meters above the bottom surface of the model soil layer.

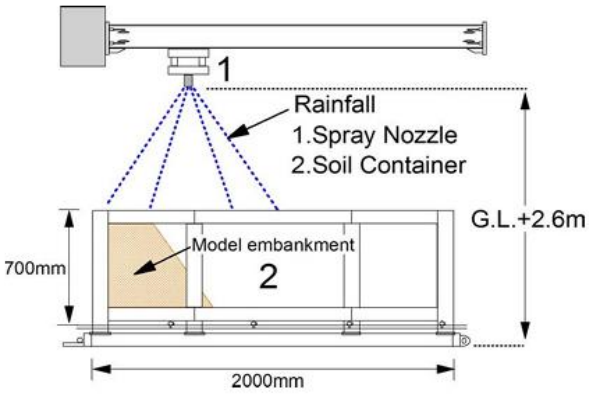

Fig. 4 Test apparatus

Furthermore, Table 2 shows the similarity law used in the model shaking table experiments [13]. This law was derived by matching the body forces that govern the mechanical phenomena of soil structures between the model (m) and the prototype (p), and it served as the basis for the discussions in this study. The scale of λ represents the ratio of the prototype to the model dimension ($1/\lambda=L_m/L_p$). Due to limitations of the experimental equipment, 1/λ is scaled to 1/8 in this study.

Table 2. Similarity law

Parameters	Scale (Model/Prototype)
Length (L)	1/λ
Time (t)	$1/\lambda^{0.75}$
Soil density (ρ)	1
Gravity acceleration (g)	1
Stress (σ)	1/λ
Strain (ε)	$1/\lambda^{0.5}$
Deformation (d)	$1/\lambda^{1.5}$
Friction (tanφ)	1
Cohesion (c)	1/λ
Permeability (f)	$1/\lambda^{0.25}$
Pore water pressure (u)	1/λ
Saturation degree (Sr)	1

Figure 5 shows the relationship between the principal stress ratio σ_1'/σ_3' and shear strain g from the consolidated undrained triaxial test (CUB test) of the Ta-d PR layer. Note that the shear strain is calculated assuming a Poisson's ratio of 0.5. As is evident from the figure, although the stress-strain relationship is

affected by the difference in adequate confining pressure (Fig. 5(a)), if normalized by the square root of σ'_c, the relationship appears to be approximately represented by a hyperbola (Fig. 5(b)). From this, the shear strength τ of the soil at collapse can be normalized by the effective confining pressure σ'_c. If the model's infiltration rate and rainfall intensity match field conditions (Ta-d has high permeability exceeding 10^{-5} m/s), then simulation of non-cohesive soil materials like Ta-d PR becomes theoretically possible.

4. MODEL SLOPE CONSTRUCTION METHOD AND TEST OVERVIEW

4.1 Model Slope Construction Method

Model slopes were prepared by air-pluviation and light compaction to achieve a target dry density of 0.442g/cm³, ensuring no particle crushing during preparation. For shaking table tests, the model slope angle was set at 45 degrees, with a preparation water content of 144.6% (natural water content) (Fig. 6). For rainfall tests, model embankments were prepared with a 70-degree slope, at which failure occurs from rainfall alone based on preliminary experimental results (45, 55, and 70-degree.), and with three initial water contents: 80%, 100%, and 110% (Fig. 7). This model experiment did not simulate the in-situ mechanical behavior, but investigated the change in the amount of particle crushing when volcanic model slopes failed. Therefore, in the model experiment, slope angles of 45-degree (in shaking table tests) and 70° (in rainfall tests) were adopted as the required conditions to collapse the slopes.

4.2 Test Overview

4.2.1 Shaking table test

For the shaking table tests, after preparing the model slope, 20 cycles of seismic loading (at 495 gal, 540 gal, and 600 gal) were applied to the model embankment to quantify the influence of these factors on slope failure. Fig. 6 shows the layout of the instruments installed within the slope. Pore water pressure was measured using pore water pressure gauges (pw1 to pw4), while saturation was monitored by dielectric soil moisture sensors (sm1 to sm6). Accelerometers were installed at the embankment's bottom, crest, and shaking table. Furthermore, sieve analyses were performed on pre- and post-test samples to confirm the presence or absence of particle crushing. The experiment was conducted at least twice, and it was confirmed that variations in ΔFc (ΔFc, %; increase rate of particles less than 0.075 mm), and pore water pressure were within 5 %. The increase rate of fines content was calculated as an index for particle crushing. ΔFc was determined by sampling soil from a 300 mm wide × 250 mm high × 20 mm deep region visually identified as the slipped area near the slip surface.

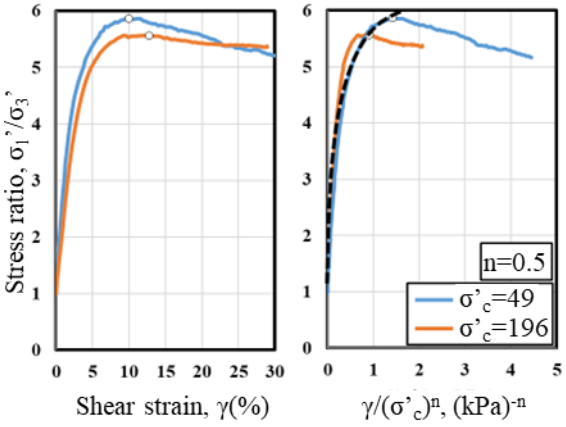

(a) (b)

Fig. 5 Stress-strain relationship

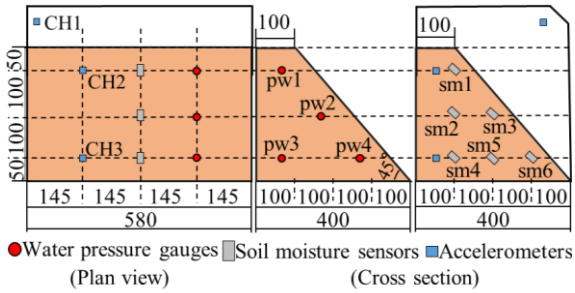

Fig. 6 Model slope shape and instrument layout (Shaking Table Test)

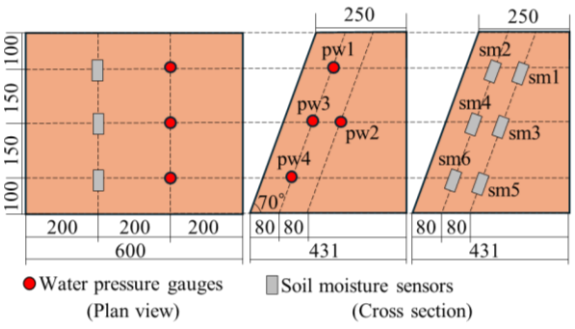

Fig. 7 Model slope shape and instrument layout (Rainfall Test)

Figure 8 typically shows the response accelerations at the accelerometer installed on the upper right of the shaking table under seismic loading (see cross-section in Fig. 6).

4.2.2 Rainfall test

A model slope was constructed on the right side of the test apparatus, and rainfall tests were performed.

The type, position, and water pressure of the spray nozzle (installed at G.L.+2.6 m) were adjusted to achieve a predetermined rainfall intensity. Previous research on other volcanic model slopes varied the rainfall intensity (60 mm/h, 100 mm/h) and confirmed no change in behavior at failure. Additionally, to investigate the change in the amount of particle crushing when the volcanic slopes failed, the rainfall intensity was set to 100 mm/h as a required condition to collapse the slopes in the model experiment. Following model slope construction, water spraying from the nozzle (Fig. 4) commenced simultaneously with measurements from pore water pressure gauges (pw1 to pw4) and soil moisture sensors (sm1 to sm6). Figure 7 shows the layout of the instruments installed within the embankment. In rainfall tests, particle crushing was assessed by quantifying ΔFc from samples collected under conditions identical to the shaking load tests. Model experiments were conducted under general temperature conditions in Hokkaido (temperature 20±5°C).

Consistent with previous research [12], slope failure was defined as the point where the average shear strain γ (%), calculated from the displacement of six inserted kite strings, reached 6% (Photo 1). This definition is supported by the findings of Kawamura and Miura (2013), who used the PIV method to monitor the failure phenomenon and found that saturation peaked when the shear strain was 4% to 6%, irrespective of the soil material, slope angle, difference in rainfall intensity, and the presence or absence of an impermeable layer; subsequently, the slope collapsed [1]. Water content changes during earthquakes and rainfall were represented by the saturation degree Sr normalized by the initial saturation Sr0 (Sr/Sr0). Furthermore, pore water pressure was evaluated using the pore pressure ratio Δu/σv'.

5. TEST RESULTS AND DISCUSSIONS

First, we investigated the pore water pressure behavior and soil moisture changes during seismic loading and rainfall, and then discussed the changes in particle crushing amount in each case.

5.1 Seismic Loading Tests

Figures 9 and 10 typically show pore water pressure behavior and saturation changes for an input acceleration of 600 gal. As shown, seismic loading increases the pore water pressure ratio. Notably, the Δu/σv′ values are large at measurement points near the slip surface (pw1, pw2, pw4). Although the saturation degree Sr at failure was relatively low (58.6 % – 62.6 %), failure is inferred to have occurred due to a rapid increase in pore water pressure caused by strong vibration.

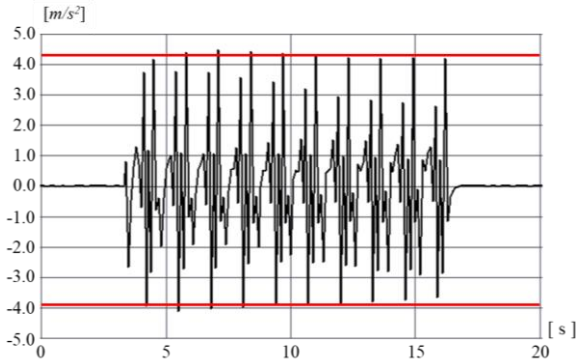

Fig. 8 Accelerations at the embankment's shaking table

Photo 1. Initial condition of the embankment side

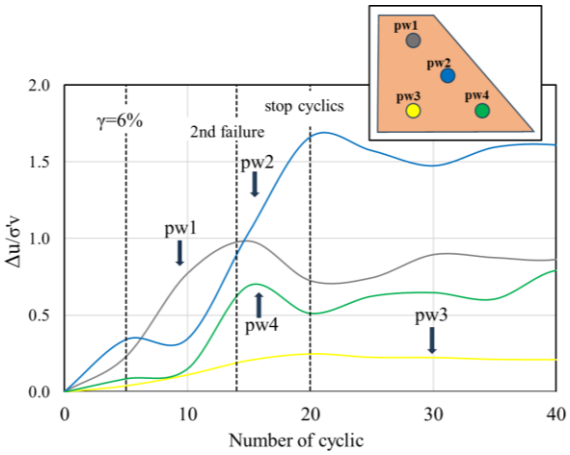

Fig. 9 Pore water pressure behavior (Shaking Table Test)

For soil moisture changes, distinct behavior was observed at measurement locations on the slip surface (sm1, sm3, sm6). This likely reflects differences in dilatancy behavior associated with the slip. Thus, it was clarified that strong vibration leads to failure even in a model ground constructed from this volcanic soil. Similar tendencies were observed for other accelerations (495 gal, 540 gal). Note that the maximum acceleration during the Eastern Iburi

earthquake in Hayakita Town, Hokkaido, which is located near this site, was 672 gal horizontally and 396 gal vertically [14].

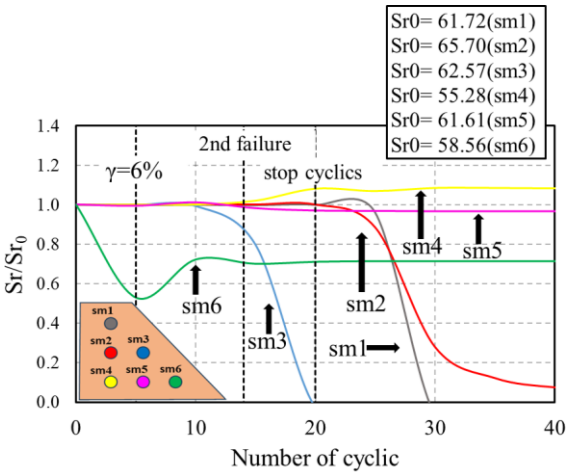

Fig. 10 Change in saturation degree (Shaking Table Test)

According to the findings presented, Fig. 11 illustrates the correlation between the acceleration of the input and the rate at which the fine content increases (ΔFc). Additionally, the figure demonstrates that the fine content has a tendency to grow as the acceleration increases. For instance, the fine content increased by 4% when the input acceleration reached 600 gal. For these samples, Fig. 12(a) shows that a 4% increase in fine content results in an increase of approximately 140 kPa in the effective principal stress according to undrained and drained triaxial test results. Similarly, Fig. 12(b) indicates that when the effective principal stress increases by 140 kPa, the internal friction angle decreases by about 8 degrees. This is in accordance with the findings of prior study [3]. Utilizing limit equilibrium analysis, we were able to arrive at an estimate of the safety factor, denoted by Fs [2]. We can write the equation as follows:

$$Fs = \frac{c+\gamma_t z cos\beta(cos\beta - k_h sin\beta \pm k_v cos\beta)tan\varphi}{\gamma_t z cos\beta(sin\beta + k_h cos\beta \pm k_v sin\beta)} \quad (1)$$

where c: Cohesion (kN/m^2), z: Depth (m), γ_t: Wet unit weight (kN/m^3), β: Slope angle (deg.), φ: Internal friction angle (deg.), k_h (=a/g): Horizontal seismic coefficient, k_v (=b/g): Vertical seismic coefficient, a: Horizontal acceleration during earthquake, b: Vertical acceleration during earthquake, g: Gravitational acceleration (gal).

According to the Japan Geotechnical Society's standards, cohesion, c for pyroclastic fall deposits such as the material used in this study should be treated as c=0 (kN/m^2). Therefore, in this analysis, the cohesion was also set to c=0 (kN/m^2), the slope angle was set to β=25° (deg.), and the depth from the ground surface was set to z=2.0m [3]. This formula is a limit equilibrium analysis. Therefore, the results obtained show the mechanical behavior at failure.

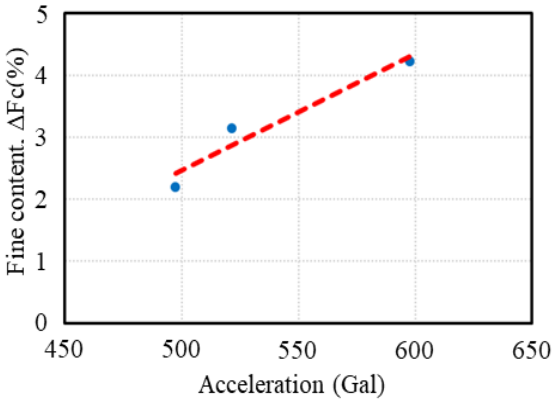

Fig. 11 Input acceleration and fine content increase rate

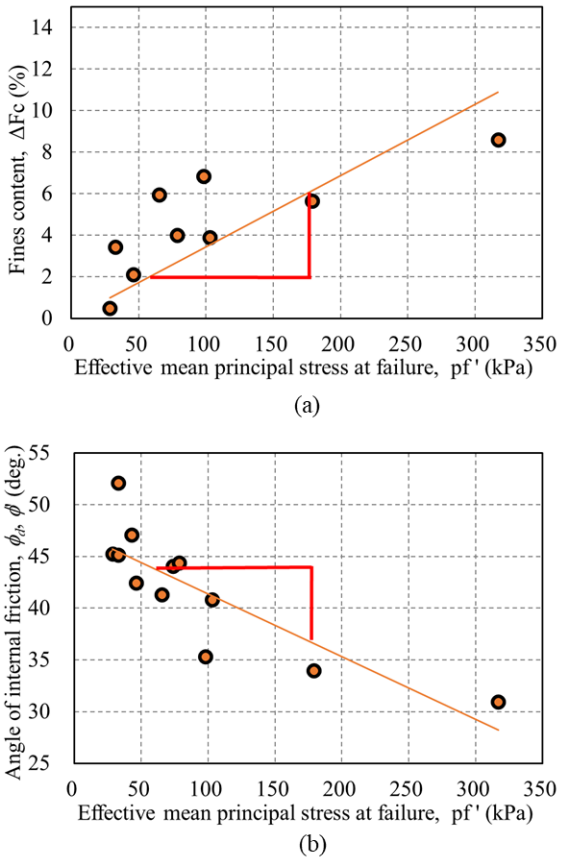

Fig. 12(a) Relationship between increment in fine-grain content and effective mean principal stress, 12(b) Relationship between angle of internal friction and effective mean principal stress

It is apparent from Fig.13 that a horizontal acceleration a=490 gal, which would result in Fs < 1, decreases to 340 gal, indicating a rapid slope destabilization.

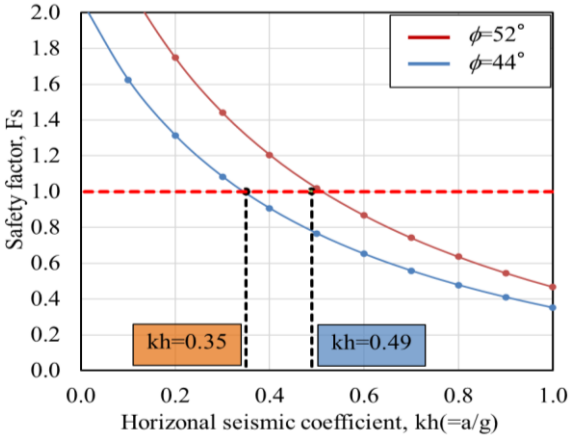

Fig. 13 Change in safety factor due to a decrease in shear resistance angle during particle crushing

These findings from unsaturated model experiments demonstrated that strong vibration and the resulting particle crushing significantly alter slope strength by reducing the shear resistance angle. The pore pressure increase in unsaturated volcanic model slopes under strong shaking is attributed to changes in the soil skeleton following particle breakage, which consequently leads to slope failure. This indicates that, even in natural slopes made of volcanic coarse-grained soil where particle crushing is common, significant cyclic shearing under seismic loading can render the slope unstable.

5.2 Rainfall Tests

Based on the findings of rainfall tests conducted with slope angles of 70 degrees and starting water contents of w_0 = 80%, 100%, and 110%, to confirm that different initial water contents cause variations in failure behavior.

Figure 14 illustrates the behavior of pore water pressure in response to rainfall events. At an initial water content of 80%, no increase in pore water pressure was observed, attributed to the low saturation state. In contrast, for initial water contents of 100 % and 110 %, an increase in pore water pressure was observed at pw1, situated at the embankment crest and identified as the potential failure location. The pore water pressure at an initial water content of 110 % was significantly elevated when γ = 6 % was attained, compared to the other two scenarios. Failure likely resulted from the rise in seepage pressure (pore water pressure) as saturation attained a steady state. Consequently, the scenario with an initial water content of 110 % reached a critical state much faster, resulting in the most unstable condition observed in the analysis.

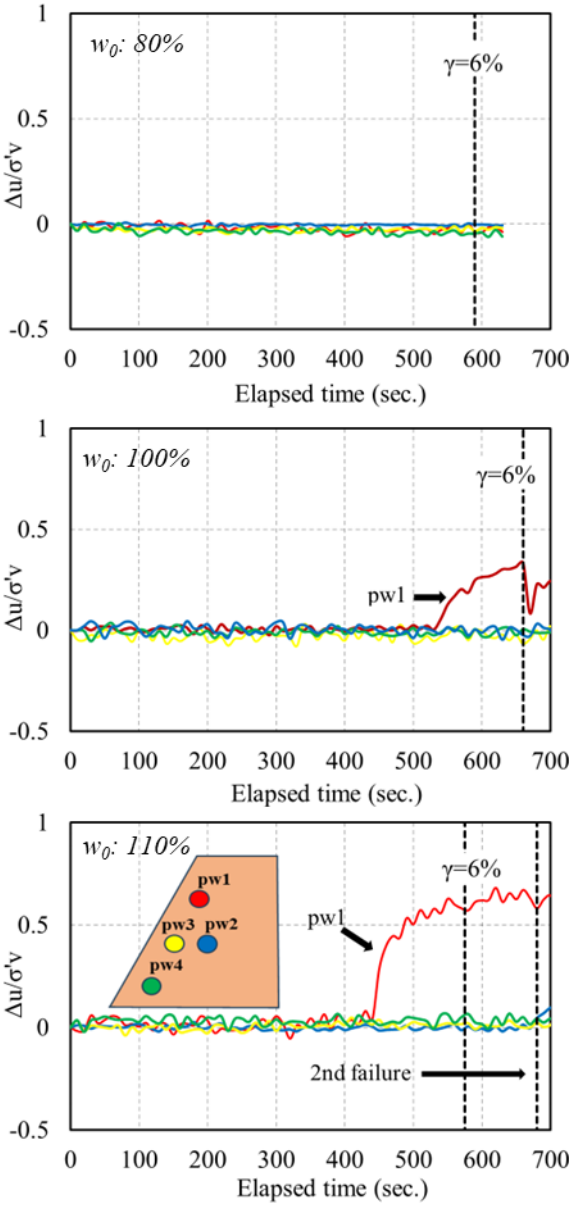

Fig. 14 Pore water pressure behavior (Rainfall Test)

Figure 15 shows soil moisture changes. While the onset time for moisture increase varied across sensors due to rainfall infiltration, an increasing trend was observed in the slope's upper and surface layers. Specifically, in the case of 80% initial water content, failure occurred across the entire slope, with sm2, sm4, and sm6 (near the failure point) showing increases. Conversely, for 100 % and 110 % initial water contents, the upper part of the slope slid down, and sm1 and sm2 showed increases. When the shear strain reached 6 %, the saturation within the embankment for sm1 and sm2 had reached mainly a steady state. Furthermore, Fig. 16 typically shows the saturation distribution within the 110 % initial water content slope, clearly indicating that rainfall infiltration increased water content in the upper and surface layers. Note that "2nd failure" indicates the

point at which a complete sliding failure occurred.

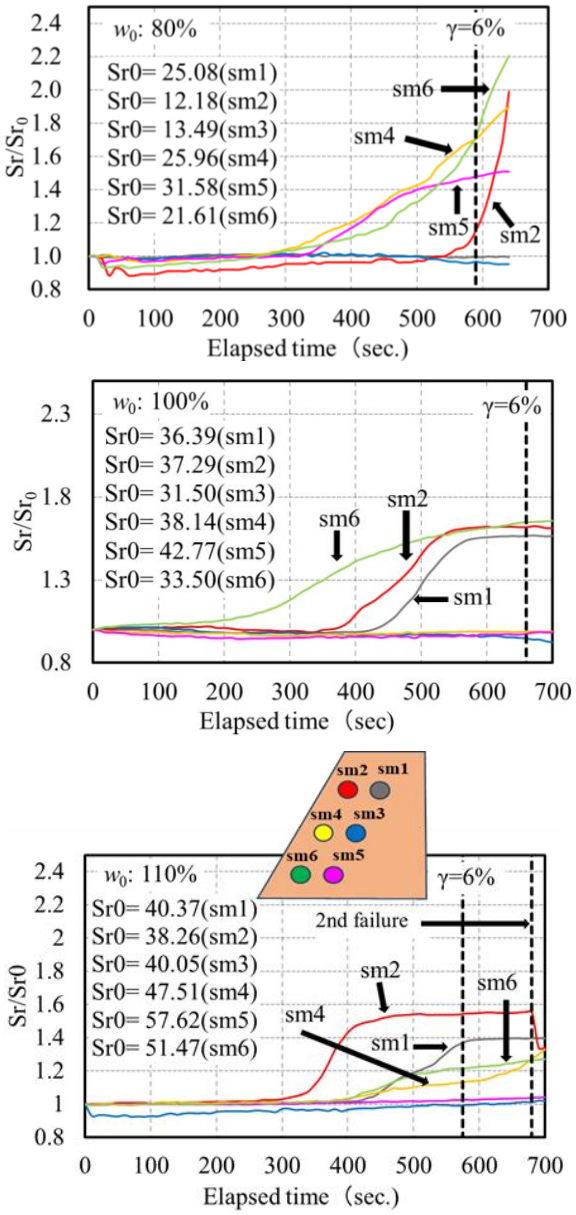

Fig. 15 Change in saturation degree (Rainfall Test)

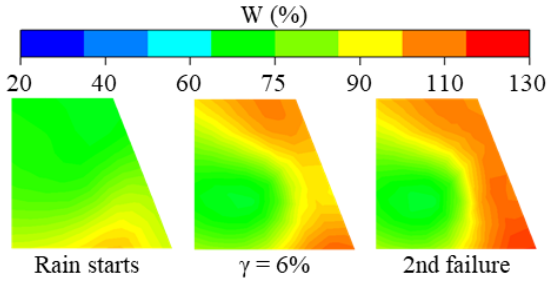

Fig. 16 Saturation distribution within embankment (Case of initial water content 110 %)

Figure 17 illustrates the relationship between the initial water content and particle crushing, revealing that the fines content increases with rising water content. Although this finding was confirmed in single-particle strength tests conducted in previous research [15], the mechanism by which these changes in soil moisture affect the overall stability of the slope remains unclear. To provide context on this effect, Ozaki (2022) investigated the failure modes of single Ta-d particles and found a significant shift: under dry conditions, 25% were compressive crushing and 75% were split crushing; this shifted to 50% compressive crushing under wet conditions [16]. This shift is likely related to microscopic voids within pumice particles. Therefore, the future research plan for this study is to clarify the governing mechanism of particle crushing, including further consideration of the strength-deformation behavior of a single particle, to fully explain the slope stability.

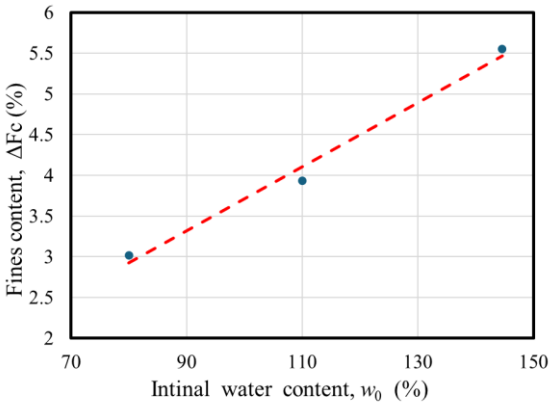

Fig. 17 Relationship between initial water content and particle crushing amount

5.3 Relationship Between Initial Water Content w_0 and Water Content at Failure w_f

Previous research [1, 12] by Kawamura et al. investigated the relationship between the initial water content (w_0) and the water content at failure (w_f) for volcanic soils in Hokkaido, proposing a unique relation that takes into account the effects of rainfall history, seismic loading history, and freeze-thaw history, irrespective of soil properties or failure modes. This relationship is expressed as follows:

$$w_f = \beta w_0^{\gamma} \qquad (2)$$

where β and γ are shape coefficients specific to the soil material.

Building on this, a similar investigation was conducted for Ta-d PR. Figure 18 illustrates the relationship between water content at failure and initial water content. The solid line in the figure represents the initial water content line.

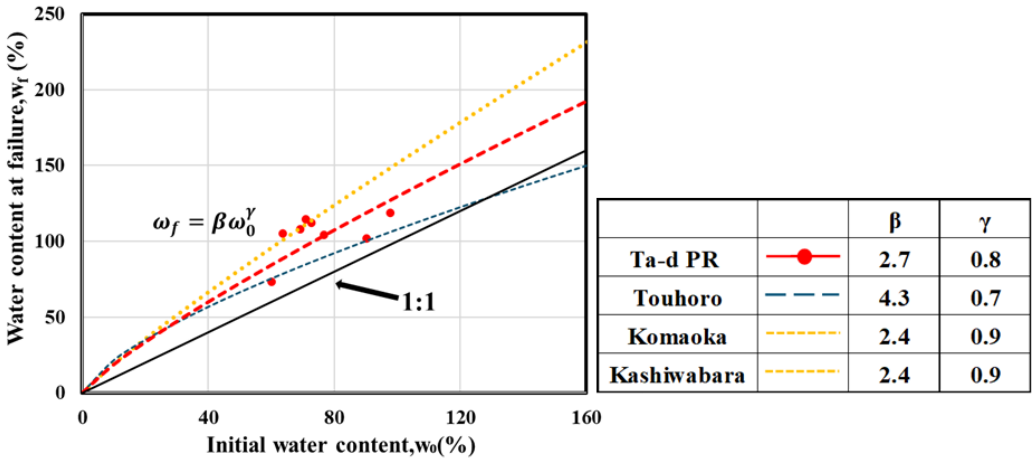

		β	γ
Ta-d PR		2.7	0.8
Touhoro		4.3	0.7
Komaoka		2.4	0.9
Kashiwabara		2.4	0.9

Fig. 18 Relationship between initial water content and water content at failure: Rainfall tests

Additionally, the figure includes results from past studies for representative Hokkaido volcanic soils: Kashiwabara (*Spfa*: Pyroclastic fall deposits), Komaoka volcanic soil (*Spfl*: pyroclastic flow deposits), and Toho volcanic ash soil (*Ma*: pyroclastic fall deposits) [1, 12]. The figure shows a unique relationship between initial water content and water content at failure in the Ta-d PR rainfall tests. Observing the approximation lines, Ta-d PR, Komaoka, and Kashiwabara volcanic soils exhibit almost similar curve shapes. Suppose a relationship (threshold) like equation (2) can be obtained for a target slope. In that case, it is believed that practical slope stability evaluation would become possible through field measurements using instruments such as soil moisture sensors. In the seismic loading test, no appreciable fluctuation in water content was detected before and after failure. This phenomenon is considered to result from a change in the soil skeleton structure induced by seismic loading, which consequently led to a decrease in the water content. Such a tendency has also been observed in other volcanic soils [15].

Currently, parallel studies are also underway to estimate soil moisture from Synthetic Aperture Radar (SAR) [17] and soil moisture estimation using machine learning [18]. If satellite SAR information or field monitoring data can be used to map soil moisture conditions over broad slope areas, and high-risk slopes can be identified based on these thresholds, it will enable discussion of specific stability for narrow-area slopes.

6. CONCLUSIONS

The following conclusions were obtained from a series of shaking table tests and rainfall tests on model slopes formed from Tarumae pyroclastic fall deposits (Ta-d-PR):

(1) In the shaking table tests, even at relatively low saturation conditions, strong vibrations induced an increase in pore water pressure, which precipitated slope failure. The reason for the increase in pore pressure in unsaturated soils under strong shaking is the changes in soil skeletons due to particle breakage.

(2) Particle crushing was observed in the model slopes of Tarumae pyroclastic fall deposits during shaking load application. This suggests that in natural slopes composed of volcanic coarse-grained soil, where particle crushing is predominant, intense cyclic shearing during seismic loadings can induce particle crushing, potentially leading to slope instability. The effect of dryness and wetness of soils depends on the minute gaps within the particles of the pumice.

(3) In the rainfall tests, it was shown that slopes failed due to rainfall infiltration, although there were temporal differences in pore water pressure development and soil moisture changes depending on the initial water content. Furthermore, the amount of particle crushing at the time of failure varied with the initial water content, being particularly more pronounced in wetter conditions. This was also confirmed in single-particle strength tests conducted in previous research [15].

(4) A peculiar relationship between the water content at failure and the initial water content emerges, forming a relation nearly identical to that obtained for typical volcanic soils in Hokkaido, Japan.

7. ACKNOWLEDGEMENTS:

This research was supported by the Hokkaido River Foundation Research Grant for FY2024, FY2025, and JSPS KAKENHI (Grant-in-Aid for Scientific Research (B), No. 24K01124). We express our sincere gratitude for their support. In addition, the authors would like to express their deep appreciation to Ms. Hikaru Kimura from Muroran Institute of Technology for her valuable assistance and cooperation in the laboratory experiments conducted during this study.

8. REFERENCES:

1. Kawamura S. and Miura S., Rainfall-Induced Failures of Volcanic Slopes Subjected to Freezing and Thawing, Soils and Foundations, 53(3) 2013, pp.443–461, DOI：10.1016/j.sandf.2013.04.006.
2. Nguyen T. N., Kawamura S., Dao M. H., and Inaba T., Influence of Fines Content on the Stability of Volcanic Embankments under Rainfall and Earthquake, Water, 14(13) 2022, p. 2096, DOI: 10.3390/w14132096.
3. Kawamura K., Matsumura S., and Kawamura S., Laboratory and Field Monitoring Tests of Volcanic Soil (Ta-d) Triggering Landslides in The 2018 Hokkaido Eastern Iburi Earthquake, Geoenviron Disasters, 11(1) 2024, DOI: 10.1186/s40677-024-00303-7.
4. Miura S., Yagi K., and Asonuma T., Deformation-Strength Evaluation of Crushable Volcanic Soils by Laboratory and In-Situ Testing, Soils and Foundations, 43(4) 2003, pp. 47–57, DOI: 10.3208/sandf.43.4_47.
5. Hyodo T., Y. Wu, and Hyodo M., Influence of Fines on the Monotonic and Cyclic Shear Behaviour of Volcanic Soil Shirasu, Engineering Geology, Vol. 301, 2022, p.106591, DOI: 10.1016/j.enggeo.2022.106591.
6. Matsumura S., Kawamura S., L. Kandpal, and P. Vangla, 3D Printed Porous Particle and Its Geotechnical Properties, Acta Geotechnica, 18(11) 2023, pp. 5735–5753, DOI: 10.1007/s11440-023-01981-7.
7. Al-Ameri, A. F. I., Jawad, F. W., Fattah, M. Y., Vertical and Lateral Displacement Response of Foundation to Earthquake Loading, International Journal of Engineering, IJE TRANSACTIONS A: Basics, 33(10) 2020, pp. 1864-1871. DOI: 10.5829/IJE.2020.33.10A.05.
8. Jawad, A. A., Hassan, W. H., and Fattah, M. Y., Finite Element Analysis of a Zoned Earth Dam under Earthquake Excitation, IOP Conf. Series: Materials Science and Engineering 1067 (2021) 012074, IOP Publishing, DOI: 10.1088/1757-899X/1067/1/012074.
9. Goto S., Influence of a Freeze and Thaw Cycle on Liquefaction Resistance of Sandy Soils, Soils and Foundations, 33(4) 1993, pp. 148–158, DOI: 10.3208/sandf1972.33.4_148.
10. Ishikawa T. and Miura S., Influence of Freeze-Thaw Action on Deformation-Strength Characteristics and Particle Crushability of Volcanic Coarse-Grained Soils, Soils and Foundations, 51(5) 2011, pp. 785–799, DOI: 10.3208/sandf.51.785.
11. Matsumura S., Miura S., Yokohama S., and Kawamura S., Cyclic Deformation-Strength Evaluation of Compacted Volcanic Soil Subjected to Freeze–Thaw Sequence, Soils and Foundations, 55(1) 2015, pp. 86–98, DOI: 10.1016/j.sandf.2014.12.007.
12. Kawamura S., Miura S., and Matsumura S., Stability Monitoring of Embankments Constructed by Volcanic Coarse-Grained Soil in Snowy-Cold Regions, Journal of Cold Regions Engineering, 35(1)2021, DOI: 10.1061/(asce)cr.1943-5495.0000240.
13. Nguyen T.N. and Kawamura S., Earthquake-Induced Failure of Volcanic Embankments Subjected to Previous Rainfall, International Journal of GEOMATE, 23(97) 2022, pp.22-30, DOI: 10.21660/2022.97.367.
14. National Research Institute for Earth Science and Disaster Resilience (NIED) Strong-Motion Seismograph Networks (K-NET, KiK-net) HP: (Kyoshin Network (K-NET, KiK-net) of National Research Institute for Earth Science and Disaster Resilience (bosai.go.jp)). [in Japanese]
15. Goto R., Kawamura S., Matsumura S. and Murakawa R., Strength Change of Tarumae Tephra Deposits Due to Drying and Wetting. The 59th Annual Conference of Japan Geotechnical Society (JGS), Asahikawa, No. 25-6-3-06., 2024. [in Japanese]
16. Ozaki H., Characteristics of crushing morphology of porous soil particles and evaluation of reproduced particle using 3D Printer, Graduation thesis, Muroran Institute of Technology, 2022. [in Japanese]
17. Ishikawa R., Kawamura S. and Izumi Y., Field Monitoring of Natural Volcanic Slopes and Its Analysis Using SAR. The 79th Annual Conference of Japan Society of Civil Engineers (JSCE), Sendai, III-124, 2024. [in Japanese]
18. Nguyen T.N., Kawamura S., Dao, M. H. and Inaba T., Effects of Fine Particles Content on Earthquake-Induced Failure of Volcanic Embankments Subjected to Rainfall, Proc. of International Conference on Geotechnics for Sustainable Infrastructure Development (GEOTEC HANOI 2023), 2023, pp. 1897-1912.